

Force-Controlled Robotic Arm Capable of Sub-Millimeter Precision – Barrett Research Project

January 15, 2010

1 Summary of the Research Performed

1. We designed and built a 4-axis WAM Arm in which the base joint (joint 1) was instrumented with a high-resolution optical encoder and read-head.
2. We ran a series of experiments to measure the accuracy of the magnetic motor encoder, the accuracy of the optical joint encoder, and the effect of cable tension on accuracy.
3. We made a conceptual design of a 4-axis WAM Arm instrumented with 4 optical joint encoders.

The rest of Section 1 of this report discusses work performed in each of the four objectives and results obtained. Section 2 summarizes problems encountered and the actions taken to resolve them. Section 3 discusses any unresolved problems. Section 4 summarizes our project results.

1.1 Objective 1: Design and build 1-axis testbed

We designed, installed, and tested Barrett's 4-axis WAM Arm with an optical joint encoder in Joint 1 (base joint). Figure 1 shows a photograph of the WAM arm and a kinematics diagram. Figure 2 is a photograph of the joint 1 pulley with added components including: optical encoder tape, encoder read-head and mounting bracket, and the encoder tape cover and cover clamp.

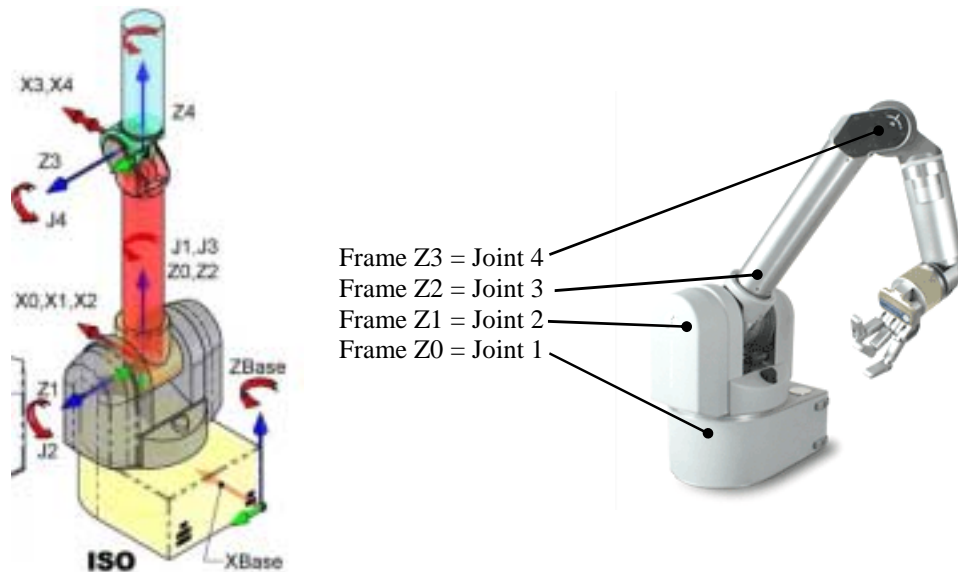


Figure 1: Image and photograph showing kinematic frames and joint locations of 4-axis WAM Arm

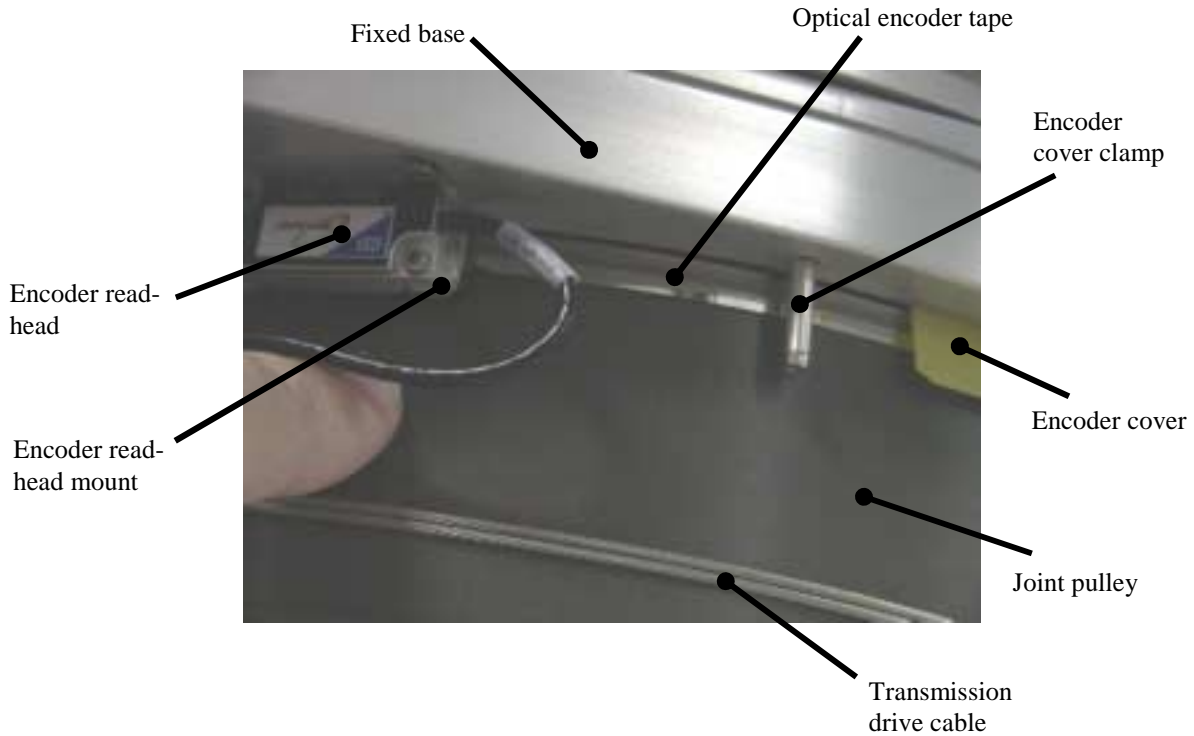


Figure 2: Photograph of single-axis testbed instrumented on Joint 1 of WAM

After assembling the system, we measured the outputs of the encoder and checked voltage levels to confirm proper alignment. Figure 3 shows the oscilloscope reading of the output of the encoder.

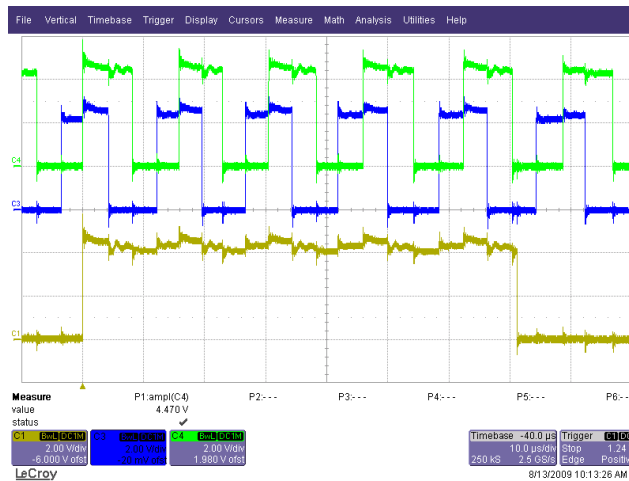


Figure 3: Oscilloscope reading of encoder showing A-pulse (green), B-pulse (blue), and Index-pulse (yellow)

We decided that a single read-head per encoder should provide the accuracy we needed. We determined that a single index pulse was adequate for our application. We examined the

tradeoffs between a housed encoder unit and a frameless one and determined that the frameless encoder was far preferable for our application. The overwhelming factor was mass. Fully housed encoders with comparable accuracy, were nearly 10x the mass of the frameless ones. We determined that scale runout should be mechanically adjusted during the alignment procedure rather than relying on software lookup tables.

1.2 Objective 2: Experiments and model development

Long-distance laser accuracy test

The purpose of this experiment was to measure the repeatability of the single-axis testbed's optical encoder and, by extension, how it would affect the positioning of the robot's endpoint.

First, we mounted a mirror on the single-axis testbed described above. Then, 120 ft away, we aimed a tripod-mounted laser at the testbed's mirror. We then used a ruler at the laser to measure the movement of the reflected dot with respect to the reported Joint 1 encoder position. Using this data, and assuming a 1 m robot using the single-axis testbed as the base joint, we determined the min, max, and average endpoint error due to the testbed's encoder to be 1.67 μm , 30.79 μm , and 18.40 μm , respectively. Table 1 shows the collected data.

Table 1: Data from long-range laser accuracy test

Encoder (cts)	Ruler (mm)	Diff (cts)	Diff (mm)	Rad (emp)	Cts (theoretical)	Err (urad)	Err@1m (mm)
414	100						
-2108	836	2522	736	0.01006	2527.48	21.83	0.02183
511	72	2619	764	0.01044	2623.64	18.47	0.01847
-2619	985	3130	913	0.01248	3135.32	21.17	0.02117
599	47	3218	938	0.01282	3221.17	12.62	0.01262
-2611	984	3210	937	0.01281	3217.74	30.79	0.03079
548	63	3159	921	0.01259	3162.79	15.09	0.01509
-2593	979	3141	916	0.01252	3145.62	18.39	0.01839
543	64	3136	915	0.01251	3142.19	24.62	0.02462
-2632	990	3175	926	0.01266	3179.96	19.75	0.01975
480	82	3112	908	0.01241	3118.15	24.47	0.02447
-2363	910	2843	828	0.01132	2843.42	1.67	0.00167
537	65	2900	845	0.01155	2901.8	7.16	0.00716
-2201	864	2738	799	0.01092	2743.83	23.22	0.02322
						Min	0.00167
						Max	0.03079
						Avg	0.01840

AS5045 magnetic runout

The error introduced by the steel cable transmission drive can only be determined once we know the errors attributable to a) the optical encoder at the joint (discovered above) and b) the AS5045 magnetic encoder at the motor shaft. Therefore, in this second experiment, we designed a platform to collect data on the angular accuracy of the magnetic encoder.



Figure 4: Motor testbed to measure 12-bit magnetic encoder accuracy

By attaching a high resolution 655360-count MicroE optical encoder to the same shaft as the 4096-count AS5045 magnetic encoder, we were able to collect data on the relative precision of the magnetic encoder. Figure 4 shows the MicroE optical encoder mounted to the top of the motor, and the motor controller with its integrated AS5045 magnetic encoder mounted below the motor. Figure 5 and Figure 6 show the difference between 2 different encoder magnet/mount assemblies.

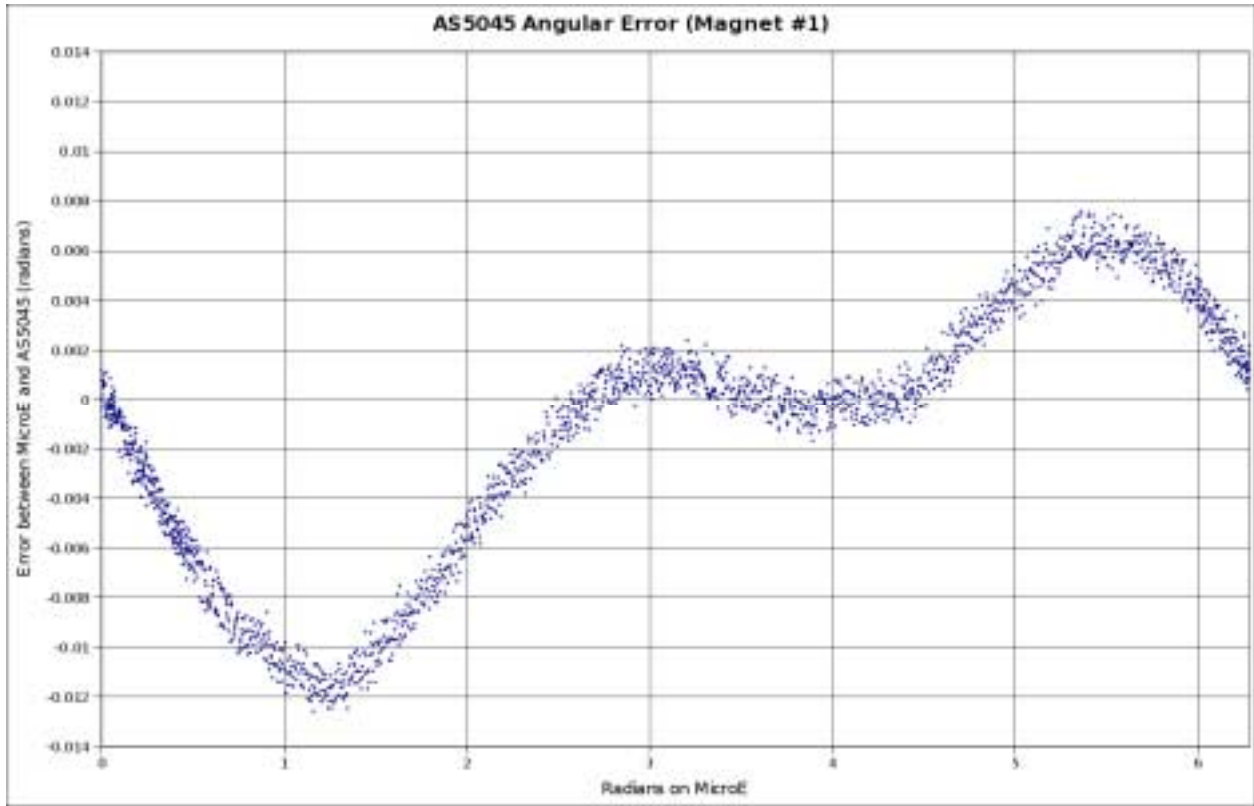


Figure 5: Plot of magnetic encoder error relative to an optical encoder for magnet spindle sample "A"

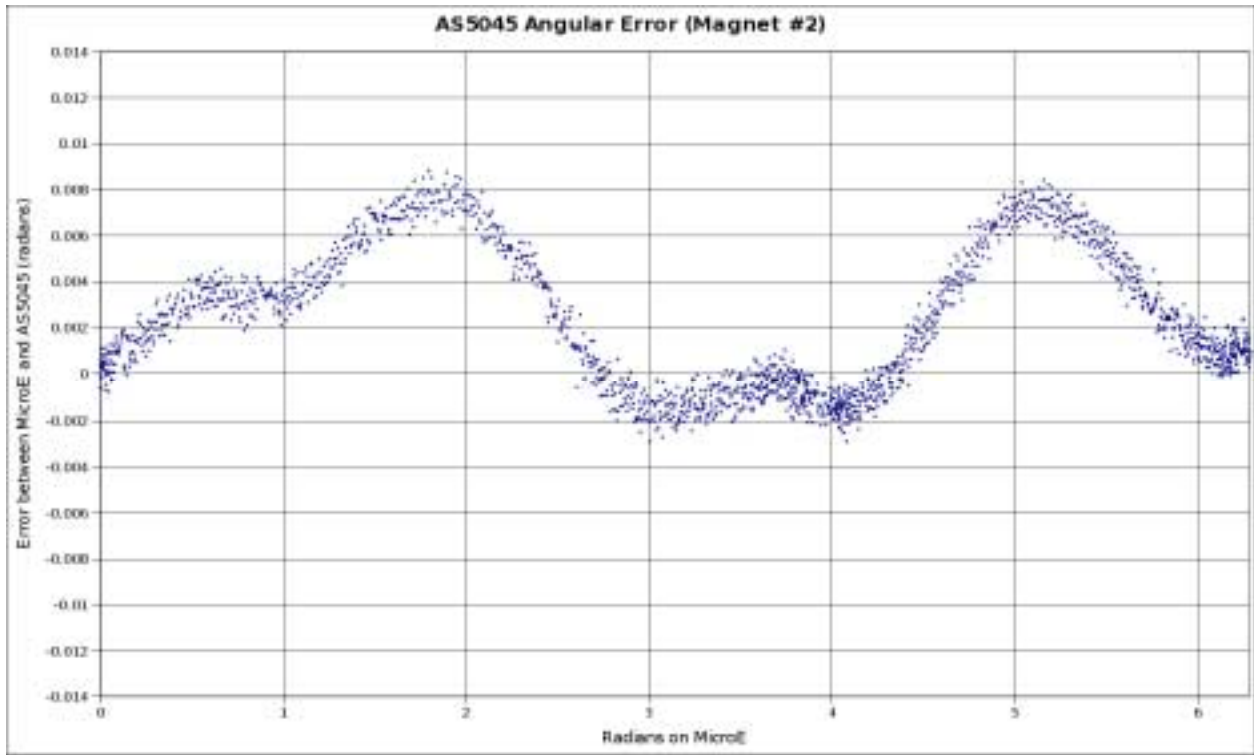


Figure 6: Plot of magnetic encoder error relative to an optical encoder for magnet spindle sample "B"

We can see that the angular error of the first magnet has a total range of about 0.02 rad (from -0.012 rad to +0.008 rad). The angular error of the second magnet has a total range of about 0.01 rad (from -0.002 rad to +0.008 rad). We can attribute this error to the magnetic run-out caused by placing the encoder magnet slightly off-center in its mount such that the magnet “orbits” around the center of the shaft. For this test, we tried to choose a poorly-placed (“A”) and a well-placed magnet (“B”), as determined by visual inspection.

Introducing the cables as a variable

Once we had determined the error attributable to the optical encoder alone and that of the magnetic encoder alone, we wanted to determine the error introduced by the steel cable transmission drive between them in our single-axis testbed. For this, we took four sets of data. First, we manually moved the joint through its range of motion in a slow teaching motion, backdriving the motor and putting low stress on the drive cables. Next we repeated this test with a fast teaching motion, putting higher stress on the drive cables. Then we had the motor drive the joint in a slow playback motion (low cable stress). Finally, we had the motor drive the joint in a fast playback motion (higher cable stress).

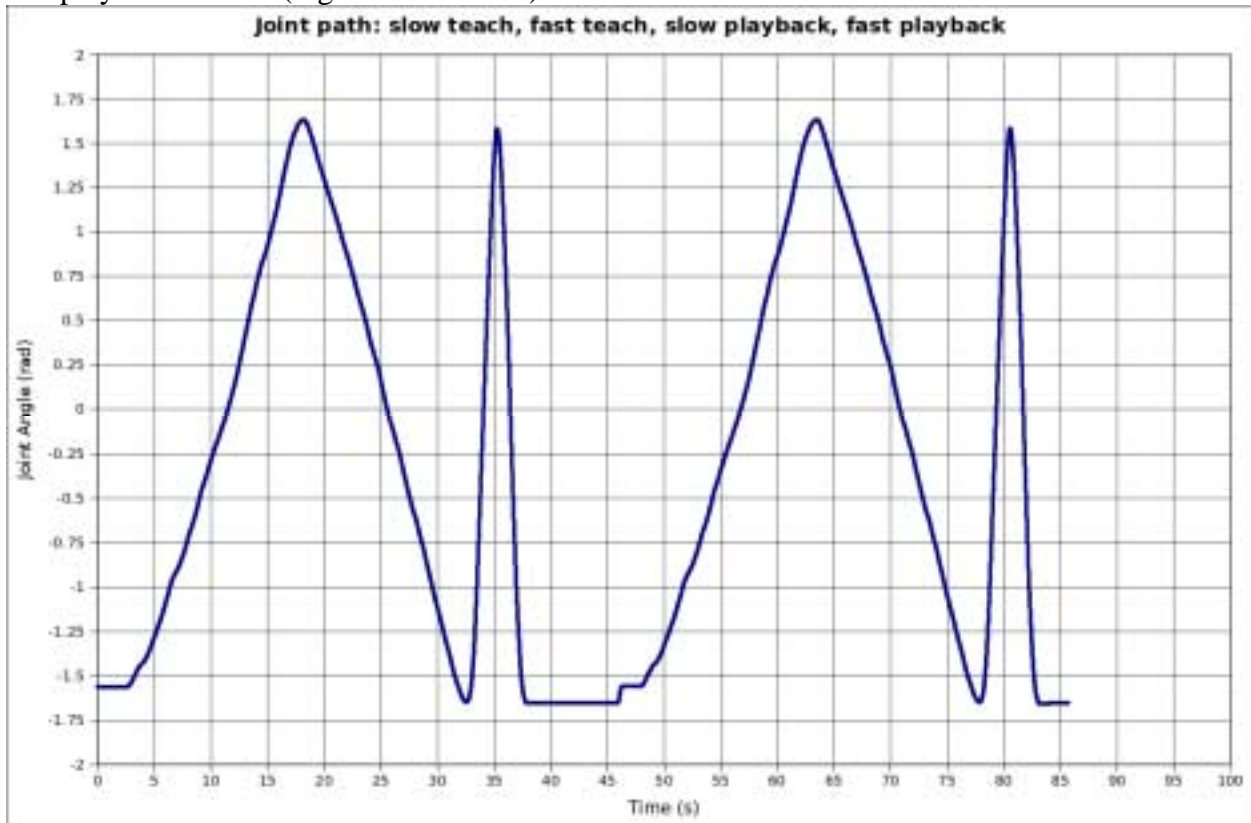


Figure 7: Plot showing the path of the joint for all four tests

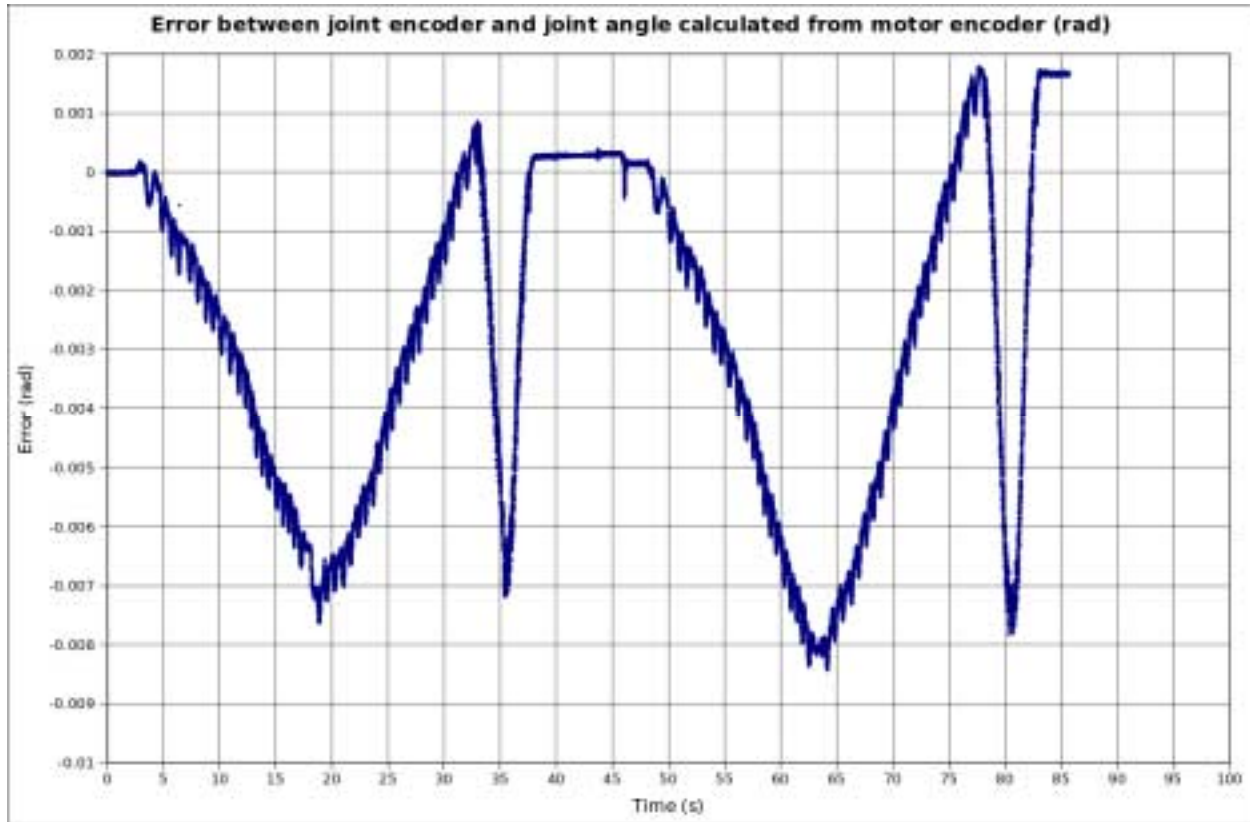


Figure 8: Error in radians vs. time introduced by the cable drives

Figure 8 shows the error introduced by the cable drives across all four tests. It is interesting to note that the error builds while moving in one direction, then it nearly returns to its initial value when the joint returns to its initial position. This phenomenon allows for high repeatability in cable drive systems while under constant load.

Taking these two figures together, we can see that the error builds up to a total of about -0.007 rad across pi rads of either slow or fast movement when the motor is backdriven by the joint. When the motor is driving the joint, the error builds up to a total of about -0.009 rad across pi rads of either slow or fast movement. In the backdriven cases (the first 2 spikes near 17 s and 36 s), the stress on the cable comes mostly from the motor’s rotor inertia as seen through the 1:42 transmission ratio. In the driven cases (the last 2 spikes near 63 s and 81 s), the stress on the cable comes mostly from the joint inertia.

The high-frequency oscillations of magnitude 0.0005 rad are as-yet unexplained. At first, we would expect that behavior to be attributable to the AS5045’s magnet orbiting in its mounting socket, but the error here is lower than the error found for the AS5045 in the previous test by an order of magnitude.

Static endpoint-force-variation testing

We performed static endpoint-force-variation testing on joint 4 of the WAM. Joint 4 has the longest section of free cable and it is not coupled to any other joints (joints 2 and 3 are coupled via a cable differential system). Figure 9 shows a plot of motor encoder error vs. mass at the endpoint of the arm. We started with 0 kg at the endpoint, then added mass in 0.1 kg increments initially, then 0.5 kg increments until we got to 4.0 kg. As the cable stretched and slack was removed from the pulleys, the motor remained stationary, but the joint moved slightly. For the final data point, we removed all added mass. Note the hysteresis in the plot. The cable was now wound more tightly on the pulleys. Also note the slight non-linearity in the plot which will complicate modeling the system.

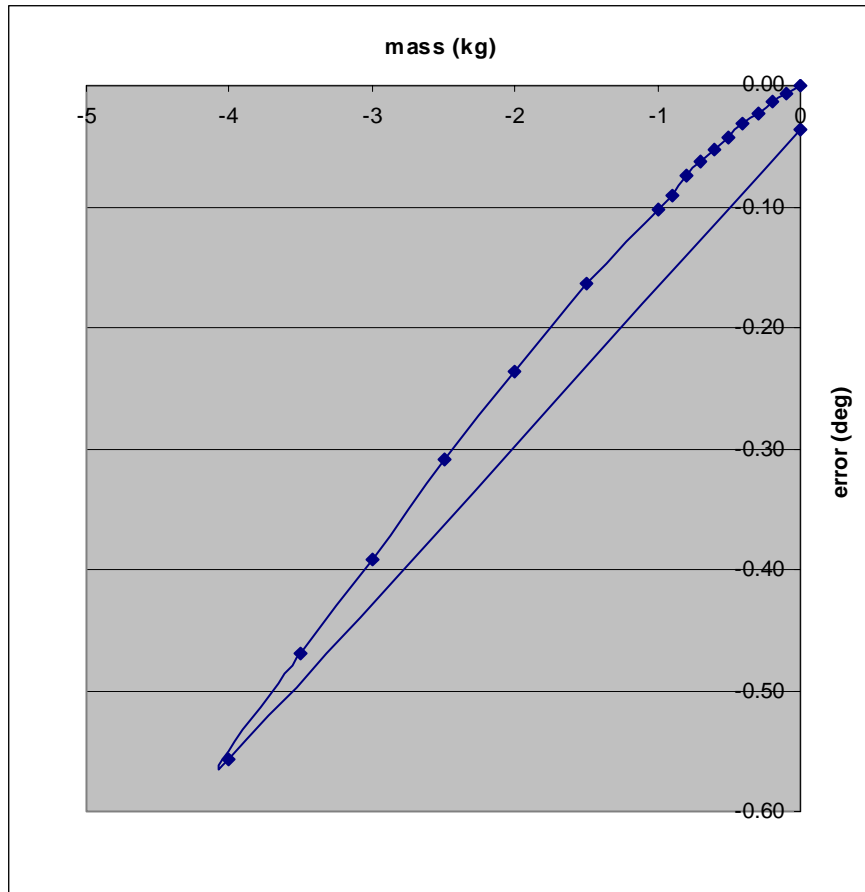


Figure 9: Plot of joint angle error vs. mass at tool plate for joint 4 of WAM

1.3 Objective 3: Conceptual multi-axis design

An analysis was performed to map encoder accuracy to toolplate location accuracy for a 4-axis WAM Arm. Commercially available optical-encoder systems were examined and chosen based on size, accuracy, cost, etc. Table 2 shows the top encoder choice for each of the four axes in the WAM and their related accuracies when used in the WAM. The encoders are from the Mercury line of optical encoders from GSI Group.

Table 2: Potential encoder models, accuracy levels, and the effects of encoder accuracy on toolplate position.

axis	encoder model	encoder accuracy based on number of counts			error at toolplate	accuracy based on total possible encoder error	error at toolplate
		<i>bits</i>	<i>counts/rev</i>	<i>urad/count</i>	<i>mm</i>	<i>urad/count</i>	<i>mm</i>
1	Merc2-tape	21	1,578,400	4.0	0.004	48.5	0.05
2	Merc1-107.95 OD	19	655,360	9.6	0.010	203.6	0.20
3	Merc1-107.95 OD	19	655,360	9.6	0.005	203.6	0.10
4	Merc1-57.15 OD	18	327,680	19.2	0.009	310.3	0.14
				Total:	0.027	Total:	0.493

This analysis formed the basis for the choice of encoder in the testbed (see Objective 1) and defined the conceptual design outlined below. Figure 10 shows a CAD model of a potential solution for adding optical encoders to joints 2 and 3 of the WAM. Shown in the model are the glass encoder discs and laser-based encoder read-heads. Figure 11 shows a potential solution for joint 4 using the same read-head, but a smaller glass disc. In all three cases, mounts would need to be designed that allowed for various adjustments for precise encoder alignment. Protective covers, wiring, alignment tools, and fixtures would be critical parts of the solution as well.

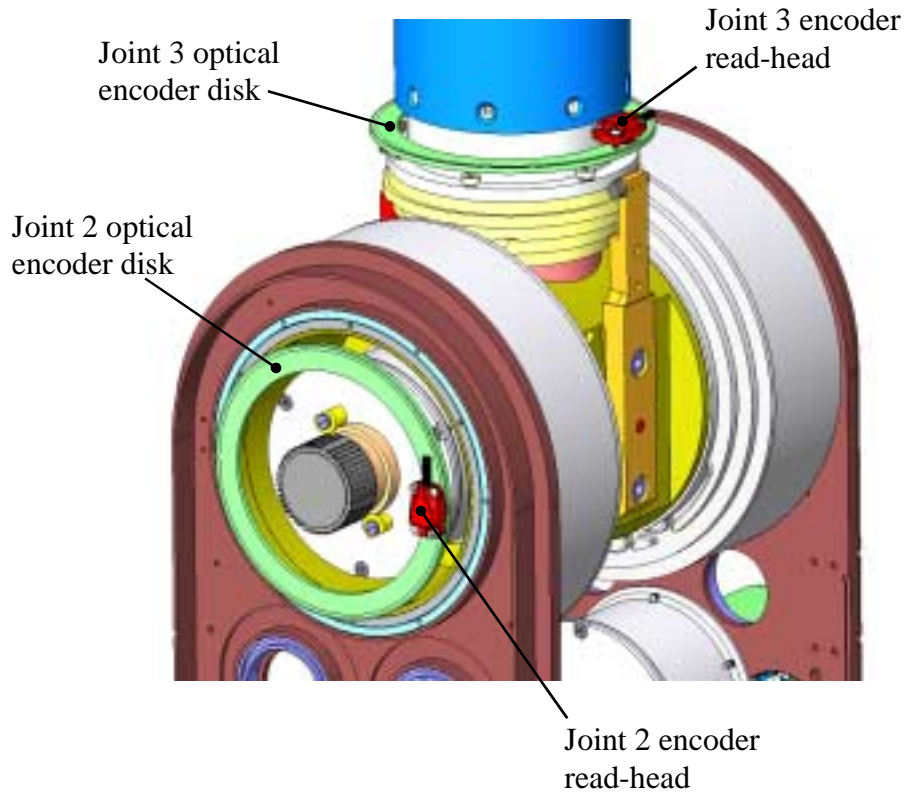


Figure 10: Conceptual design of optical joint encoders at joints 2 and 3 of the WAM Arm

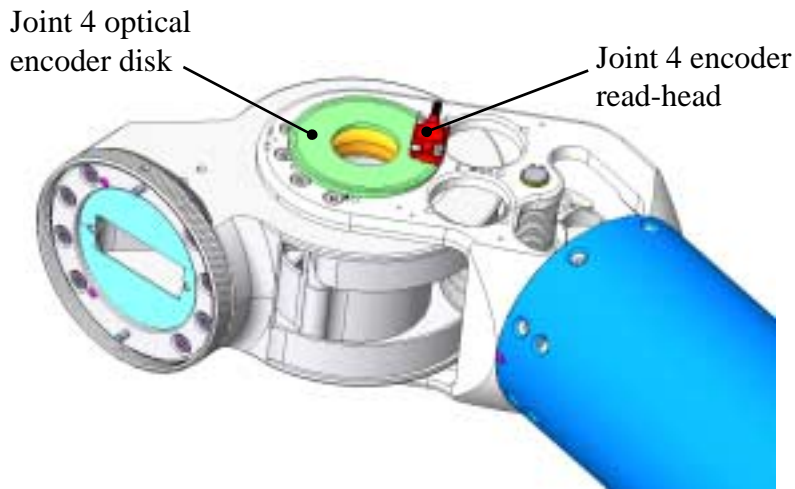


Figure 11: Conceptual design of an optical joint encoder at joint 4 of the WAM Arm

In response to the questions posed in our proposal, it was determined that two of the four joints could use the same glass disc (joints 2 and 3) and three of the joints could use the same read-head (joints 2,3,4). Joint 1 requires the use of optical metal tape and thus requires a different read-head. By using some of the same components in at least more than one joint, we can save on cost. The results of Objective 2 show that while there may be some added benefit to modeling

cable stretch and varying joint location based on the model, a joint encoder will be far more reliable and accurate.

2 Resolved Problems and Lessons Learned

Joint 1 encoder installation

The metallic optical tape used on the joint 1 pulley was difficult to install without proper fixtures. After several failed attempts, we designed and made fixtures to help align the tape to the pulley and align the read-head to the encoder tape. It is likely that the encoder at each joint will require its own set of special tools, fixtures, and procedures.

Encoder feedback via Barrett's Puck motor controllers

We underestimated the difficulty and work involved in using our Puck motor-control module to read and process the data from the optical encoder *while* performing all of its other functions *and* being cross-compatible with our other products. We had to revise the bill of materials of the Puck and change our in-house testing procedures to accomplish this. The Puck can now read data simultaneously from two different encoders while controlling current to three motor phases of a single brushless motor. When a Puck is installed in a WAM with joint encoders, it will read the 12-bit magnetic encoder on the motor and the 18+ bit optical encoder on the joint.

3 Unresolved Problems

The high-frequency angular error in Figure 8 looks like a magnet orbiting on the motor shaft as it is read by the AS5045 magnetic encoder, but its error amplitude is low by a factor of 10 based on the data collected in the AS5045 magnetic runout tests. It is possible that this magnet was particularly well-placed in its mount. Or perhaps the error can be attributed to discrete sampling errors, given the extreme difference in resolutions between the motor and joint encoders. We will need to study this matter more thoroughly in order to make a formal conclusion.

4 Conclusions

In this project we successfully installed an optical encoder onto the base joint of Barrett's WAM Arm. Analysis and testing showed that the accuracy of the arm increased significantly. The additional cost and complexity of adding joint encoders is reasonable relative to the overall cost of the system. While we were able to measure cable stretch and sag and quantify it for some different cases we felt that it would be prohibitively complex to model the cable dynamics fully given the number of varying parameters throughout the system (length of free cable between pulleys, initial tension of the cable, twist in the cable, gravity vector relative to moving joints, temperature, etc). While simpler models may slightly improve accuracy, in order to improve accuracy significantly we will need to install joint encoders on at least the additional three joints of a 4-axis arm. Even greater accuracy could be achieved by adding joint encoders to one or more of the three axes in the Wrist module that attaches to the WAM Arm. We will also need to develop a comprehensive system-level calibration routine with special tools that allow each 4-axis and 7-axis WAM to be individually factory-calibrated prior to shipment.